

Monoenergetic Proton Radiography of Inertial Fusion Implosions

Identification and characterization of the physical phenomena associated with dynamic, extreme states of matter, such as those of high-energy-density physics^{1,2} found in inertial fusion,^{3,4} laboratory astrophysics,^{2,5} and laser–plasma interaction physics,⁶ are of fundamental scientific importance. A unique method of diagnosing inertial fusion implosions has resulted in the characterization of two distinct electromagnetic field configurations that have potentially consequential effects on implosion dynamics. This method also makes possible the quantitative study of the temporal evolution of capsule size and areal density.

The method involves radiography using a pulsed (0.1 ns), monoenergetic (15.0 MeV), quasi-isotropic proton source.⁷ Fields are revealed in radiographs through deflection of proton trajectories, and areal densities are quantified through the energy lost by protons while traversing the plasma. The imaged samples are inertial confinement fusion (ICF) capsules of the fast-ignition (FI) variety,^{8,9} initially 430 μm in radius, imploded by 36 laser beams that deposit 14 kJ of energy in a 1-ns pulse (see the appendix, p. 51).

For electricity generation^{3,4} and for studies of high-energy-density physics in the laboratory,^{1,2} ICF seeks to release copious energy by igniting a compressed pellet of fusion fuel. Fuel compression to densities of 300 g/cm^3 or higher will be achieved by energy deposition onto the surface of a fuel capsule over nanosecond time scales, either by laser light (direct drive) or by x rays generated in a cavity by laser light (indirect drive). Ignition and energy gain will occur in a central hot spot or, in the FI scheme, by the extremely rapid (\sim picoseconds) deposition of additional energy, either directly onto the compressed pellet,⁸ or along the axis of a cone that keeps the path clear of plasma ablated from the pellet surface.⁹

The 15-MeV, monoenergetic proton radiography applied herein was recently used by Li *et al.* in a different context to investigate fields generated by laser–foil interactions.^{10,11} MacKinnon *et al.*¹² used a broadband, non-isotropic proton source to study six-beam implosions, although they did not observe either striated or coherent field structures. In addition,

earlier workers, using optical techniques largely sensitive to density perturbations, observed very fine-scale radial filaments and jets^{13,14} in targets driven by one to four laser beams. However, the character of these structures is qualitatively different in several ways from the striations described in this article (see the appendix, p. 51).

In the experiments reported here (Fig. 113.47), cone-in-shell FI targets were radiographed before and during implosion, 1.56 ns after the start of the laser drive (Fig. 113.48), shortly after the end of the acceleration phase.⁴ The radiographs were taken perpendicular to the Au cone axis. Figure 113.49 shows the experimental results (which are also characteristic of many implosions without cones). Because the detector records proton fluence and energy, Fig. 113.49 shows images that illustrate the spatial distributions of both proton fluence and mean proton energy.

Five important features are apparent in these images: First, the character of the isotropic and monoenergetic proton source

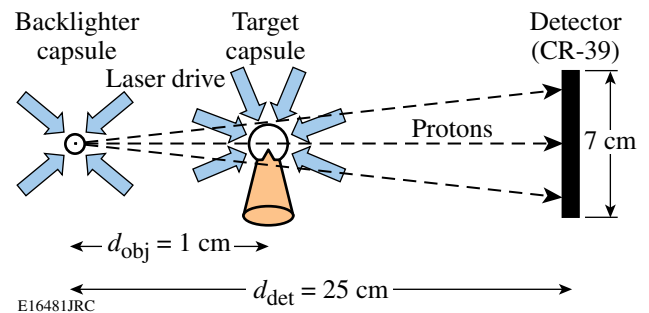


Figure 113.47 Schematic of experimental setup. A short (130 ps), monoenergetic ($\Delta E/E < 3\%$), quasi-isotropic pulse of 15.0-MeV D^3He fusion protons is generated by laser implosion of a backlighter capsule filled with D_2 and ^3He gas. The $\sim 3 \times 10^8$ protons emitted from the 45- μm FWHM source region interact with matter and electromagnetic fields in a cone-in-shell capsule implosion. The position and energy of every proton reaching the detector are individually recorded on CR-39, encoding the details of the matter and field distributions surrounding the target capsule.

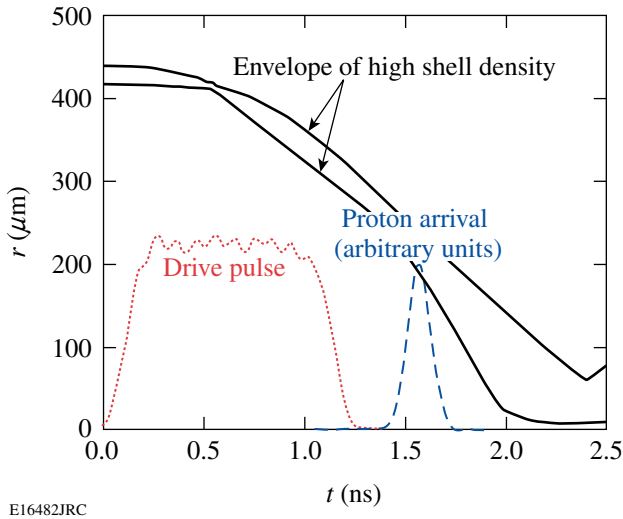


Figure 113.48

Cone-in-shell capsule drive pulse (dotted), simulated¹⁶ shell trajectory (solid), and experimental backlighter proton arrival time (dashed). Simulations predict that the shell has compressed from its original radius by about a factor of 2, and the ρR has doubled to 5 mg/cm^2 when the backlighter protons arrive at 1.56 ns (OMEGA shot 46529).

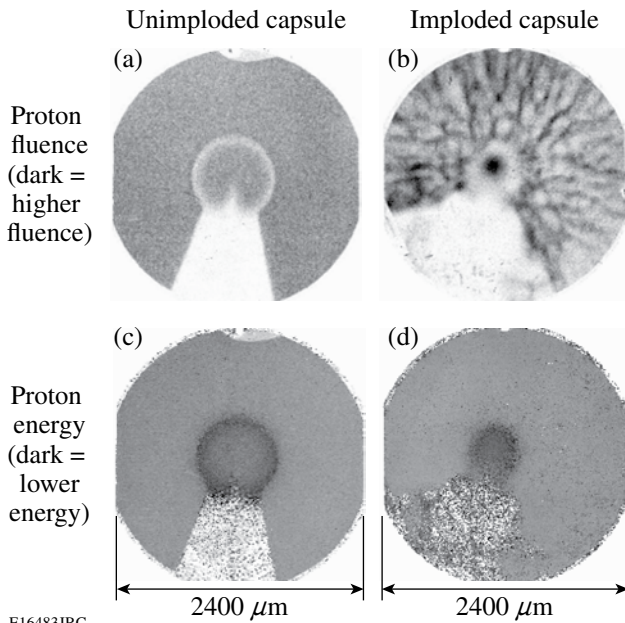


Figure 113.49

Images of a $430\text{-}\mu\text{m}$ -radius spherical CH capsule with attached gold cone, before and during implosion. Images (a) and (c) show the unimploded capsule used in OMEGA shot 46531. Images (b) and (d) show a capsule at 1.56 ns after the onset of the laser drive (shot 46529). In (a) and (b) dark areas correspond to regions of higher proton fluence, and in (c) and (d) dark areas correspond to regions of lower proton energy. The energy image values in the region shadowed by the cone are mostly noise since very few protons were detected in that region. See lineouts in Figs. 113.50 and 113.52 for image values.

is reflected in the uniform background of Figs. 113.49(a) and 113.49(c). Second, a complex filamentary structure is seen in the fluence image of Fig. 113.49(b). The uniform energy seen outside the capsule in Fig. 113.49(d) demonstrates that the fluence striations are caused by electromagnetic deflection rather than scattering through plasma density filaments. Third, substantial plasma blowoff from the cone casts a much wider shadow as the capsule is imploded. Fourth, a significant enhancement of the proton fluence at the center of the imploded target [Fig. 113.49(b)] suggests the presence of a radially directed, focusing electric field. Finally, radial compression of the capsule by a factor of 2 is seen in Fig. 113.49(d). The basic repeatability of the field structure and capsule compression was demonstrated using radiographs taken at the same relative time, but on different implosions.

In the images, field structure is studied by means of the spatial distribution of proton fluence. The proton-path-integrated electric (E) or magnetic (B) field can be estimated from the angular deflection θ of protons of energy E_p passing through the field region:

$$\int E_{\perp} d\ell = 2(E_p/e)\tan\theta, \quad (1)$$

$$\int \mathbf{B} \times d\ell = (m_p v_p/e)\sin\theta, \quad (2)$$

$$\tan\theta = M\xi/(d_{\text{det}} - d_{\text{obj}}), \quad (3)$$

where m_p is the proton mass, v_p is the proton speed, e is the fundamental unit charge, the magnification $M = 25$, and d_{det} and d_{obj} are defined in Fig. 113.47. The deflection angle is determined by measuring the apparent displacement ξ of protons in the target plane using Eq. (3).

Areal density at different positions in the target capsule is studied through the downshift in proton energy relative to the incident energy of 15.0 MeV. It is proportional to the amount of matter traversed between the source and detector,¹⁵ quantified by $\rho L (= \int \rho d\ell)$.

Radial lineouts of the images in Fig. 113.49 are shown in Fig. 113.50. In the fluence lineout [Fig. 113.50(b)] for the imploded target, the value near $r = 0 \mu\text{m}$ is strikingly enhanced relative to the values at large radii (by a factor of 3) and at $r = 200 \mu\text{m}$ (by a factor of 6). To explain this, a radial electric field of about $1.5 \times 10^9 \text{ V/m}$ is necessary to “focus” 15.0-MeV protons passing near $r = 200 \mu\text{m}$ toward the center to the extent observed. Scattering is insufficient to explain this result (see Fig. 113.51).

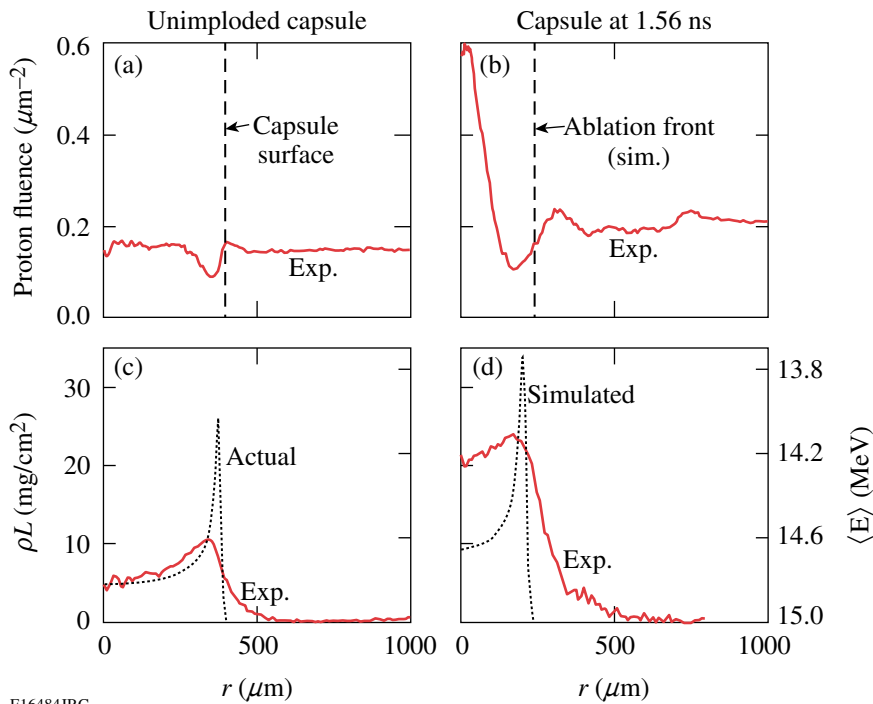
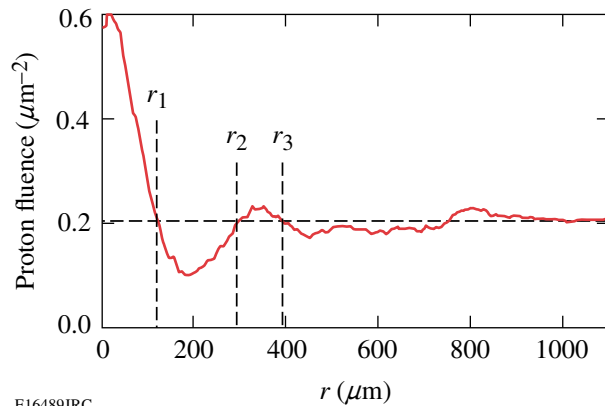


Figure 113.50

Radial lineouts of proton fluence and mean-path areal density (ρL) from Fig. 113.49. All lineouts are averaged over the azimuth, excluding the region of the cone shadow. (a) and (c): Unimploded capsule of shot 46531; (b) and (d): capsule of shot 46529, 1.56 ns after start of laser drive. The fluence lineout (a) shows the effects of angular scattering through the limb of the capsule shell. In (b), angular scattering effects alone are insufficient to explain the peak at $r = 0$. A radial electric field of $\sim 10^9$ V/m is necessary to “focus” the protons to the extent observed. In (c) and (d) radial lineouts of the mean energy images in Fig. 113.49 were converted to ρL . Also displayed are the (c) actual and (d) simulated ρL , assuming no angular scattering (dotted), where $\rho L/2 = \rho R$ at $r = 0$.

E16484JRC



E16489JRC

Figure 113.51

Reproduction of Fig. 113.50(b), marking the boundaries of the proton fluence enhancement at the center ($r < r_1$), the fluence depression through the capsule limb and E-field region ($r_1 < r < r_2$), and a secondary fluence enhancement outside the shell ($r_2 < r < r_3$). Fluence peaks and troughs in the far-field region ($r > 430 \mu\text{m}$ = initial capsule radius) are the result of filamentary structures. Also marked is the proton fluence of $0.20 \text{ protons}/\mu\text{m}^2$, equal to the far-field average fluence. In the absence of a focusing electric field, one would expect that scattering of protons through the capsule limb should deflect an approximately equal number of protons inward as outward. The number of protons deflected out of the trough region $r_1 < r < r_2$ is about 12,300, calculated as the difference in the number of protons over an azimuthal integral in that region compared to the expected number based on the far-field fluence and the area of the region. The number of protons deflected into the inner and outer proton fluence peaks are 8200 and 4100, respectively. Therefore, angular scattering through the limb plasma can account for only about half of the protons in the central peak; we invoke the presence of a focusing E field to explain the remainder of the fluence enhancement at the center.

We conjecture that this coherent field is a consequence of a large, outward-directed electron pressure gradient that exists in the vicinity of the fuel–shell interface. Such a field might be expected to occur during, and shortly after, the acceleration phase of the implosion in which substantial shell mass is rapidly assembled and compressed. Such an electric field, given by $-\nabla P_e/en_e$, has been observed in the context of other recent laser–plasma experiments.¹⁰ In this case, future measurements of the evolution of this coherent E field might effectively map capsule pressure dynamics throughout the implosion. Such information would be invaluable in assessing implosion performance.

Lineouts of the mean energy images of Figs. 113.49(c) and 113.49(d) can be used to infer the mean-path areal density ρL , shown in Figs. 113.50(c) and 113.50(d). The ρL lineout [Fig. 113.50(c)] of the unimploded target gives an initial radial areal density (ρR) of $2.5 \text{ mg}/\text{cm}^2$, which is very close to the actual initial ρR of $2.4 \text{ mg}/\text{cm}^2$. Scattering of protons smears out measured ρL values near the limb of the shell at $r = 410 \mu\text{m}$. Both measurement and simulation¹⁶ indicate a factor-of-2 reduction in capsule radius at 1.56 ns. However, the ρL lineout [Fig. 113.50(d)] of the imploded capsule at 1.56 ns implies that the capsule ρR has increased to $10 \text{ mg}/\text{cm}^2$, which is twice the $5 \text{ mg}/\text{cm}^2$ predicted by numerical simulation. This high apparent experimental ρR is due in part to scattering and in part to E-field focusing of the lower-energy protons passing through the limb of the capsule shell.

Returning to the filamentary fields, we note how the outer edge of the coherent field merges, at a boundary just outside the imploding capsule, into the striated fields. As illustrated in Fig. 113.52(c) and in Fig. 113.55 of the appendix, the striated fields originate inside the critical surface, which is extremely close to the capsule surface. Azimuthal lineouts of the proton fluence image of Fig. 113.49(b) at radii 430 μm and 860 μm show the amplitude and scale of proton fluence variations (Fig. 113.52) due to striations. Peak-to-valley fluence modulations of a factor of 4 are seen at both radii. The typical angular oscillation period is 20° and 10° for the inner and outer radii, respectively, corresponding to the same 150- μm spatial distance between striations. This distance implies a deflection angle of 0.45° , which gives a path-integrated magnetic field $\int \mathbf{B} \times d\ell$ of 4000 T μm . Assuming an integration path length equal to the typical width of striations (75 μm) results in a magnetic field strength of ~ 60 T. If the fluence variations are instead due to E fields, the field strength required is $\sim 3 \times 10^9$ V/m, although quasi-neutrality of the coronal plasma with no laser energy source makes this interpretation unlikely.

The occurrence of such strong inhomogeneities inside the critical surface ~ 0.5 ns after the laser drive ends suggests that substantially larger fields are likely present just before laser shutoff.^{17,18} This situation would be reflected in a Hall parameter ($\omega\tau$) of the order of 1 or larger, the inverse square of which reduces the classical electron heat transport.^{17,18} This situation

would result in the inhomogeneous inhibition of thermal transport over the capsule surface, altering even the zeroth-order hydrodynamics.^{18,19} Whether the source of these inhomogeneities is Rayleigh–Taylor (RT),²⁰ electrothermal,¹⁹ collisional Weibel,^{13,17} or another instability, they will provide seeds for RT growth that, if too substantial, could degrade capsule compression and quench ignition during the final stagnation phase.^{4,17,18} These issues are being actively investigated.

It seems plausible that either the electrothermal or RT instability could be the relevant source. Ongoing planar experiments, in which RT was purposely seeded, measured B fields of the order of 100 T using the method described here (see the appendix, p. 51). Furthermore, estimates (based on Ref. 18) of the RT-generated B field under similar conditions give fields of the same magnitude (see the appendix, p. 51). Radiography of driven solid-CH balls, which undergo no acceleration to drive RT growth, could be used to determine if RT is a contributing mechanism.

Finally, the vast spatial extent of these striated fields likely reflects their outward convection resulting from the plasma flow because the fields are tied to the out-flowing plasma due to high plasma electrical conductivity. We conjecture that these radiographic images thus provide snapshots of structures originally produced inside the critical surface at various times during the implosion.

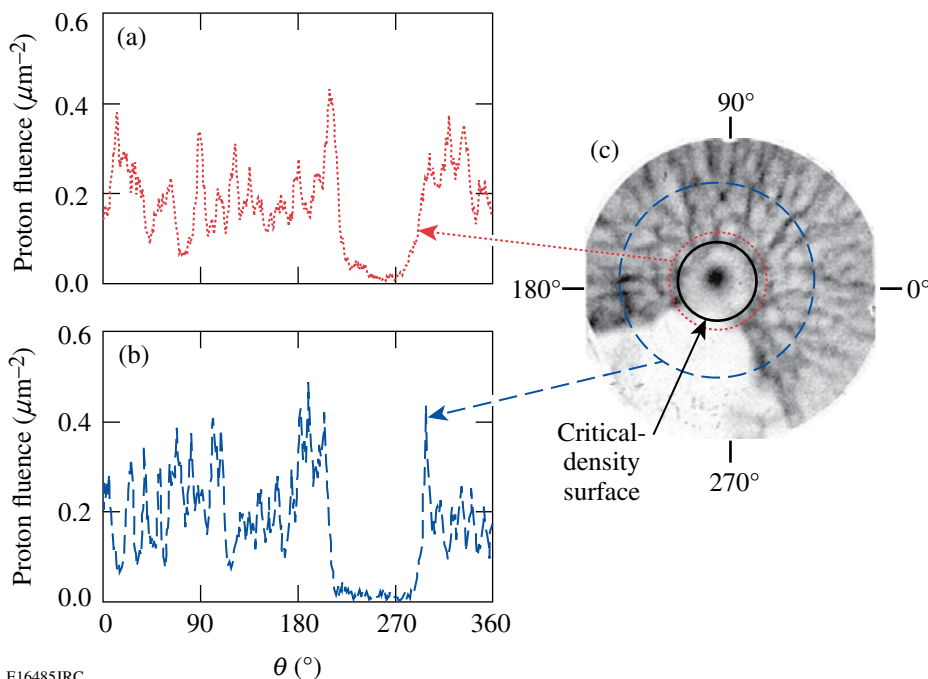


Figure 113.52

Circular lineouts of proton fluence obtained from shot 46529 at radii of (a) 430 μm and (b) 860 μm . The filamentary structures represent a 2-D projection of a 3-D field structure that originates inside the critical density surface (c).

E16485JRC

In summary, two distinctly different, simultaneously occurring electromagnetic field structures, with important implications for implosion dynamics, have been characterized in imploding ICF capsules. First, a complex filamentary field topology permeates the entire 2400- μm field of view with striations corresponding to 60-T magnetic fields. This field, through the inhomogeneous inhibition of heat flux in the vicinity of the ablation surface, could generate seeds for RT growth, thereby affecting the overall implosion dynamics.^{4,6,18,19} Second, a coherent, radial electric field of magnitude 10^9 V/m exists in the immediate vicinity of the capsule, dramatically focusing protons toward the center.²¹ This hitherto unobserved field is conjectured to originate from the gradient of electron pressure. If verified, a window for analyzing the evolution of the internal pressure dynamics is opened; this would be of immense value for critically assessing the entire implosion process.

Appendix: Monoenergetic Proton Radiography of Inertial Fusion Implosions

1. Materials and Methods

All experiments were performed at the OMEGA Laser Facility,²² which delivers up to 30 kJ in 60 beams at a wavelength of 351 nm. Full beam smoothing²³ was used on each beam to reduce high-mode nonuniformities caused by laser speckle.

A schematic illustration of the proton radiography setup is shown in Fig. 113.47. The source of monoenergetic protons is a 220- μm -radius, 2.2- μm -thick spherical glass (SiO_2) shell filled

with deuterium (D_2) and helium-3 (^3He) gas.⁷ This backlighter capsule is illuminated by 17 laser beams, delivering 6.9 kJ of energy in a 1-ns pulse, which compresses and heats the gas such that the $\text{D}-^3\text{He}$ fusion reaction, $\text{D} + ^3\text{He} \rightarrow ^4\text{He} + \text{p}$, proceeds. The protons are quasi-isotropically emitted in a 130-ps pulse²⁴ at an energy of 15.0 MeV²⁵ with a spectral width²⁶ $\Delta E/E < 3\%$ and from a region 45 μm across⁷ (see Fig. 113.53). Typical proton yields are 1 to 4×10^8 , and the yields for the OMEGA shots shown in the manuscript were 2.9×10^8 (shot 46531) and 3.7×10^8 (shot 46529). The backlighter implosion has not yet been fully optimized for proton yield, pulse duration, or source size.

The target imaged is a 430- μm -radius, 23- μm -thick spherical plastic (CH) shell with an embedded gold (Au) cone of 5-mm height, 30- μm thickness, and an opening angle of 35° . The cone ends in a shelf (see Fig. 113.54) where the cone intersects the shell, and a smaller cone tip reaches inward to a distance of 40 μm from the capsule center. Forty beams in a spherically symmetric configuration are pointed at the spherical shell; the shell is then directly driven with 14.1 kJ using 36 of those beams (the four beams aimed nearest the cone axis remain off to avoid the laser hitting the inside of the cone), for an on-target illumination intensity of 6.7×10^{14} W/cm². Because the OMEGA system is optimized for a 60-beam spherical drive, the illumination uniformity is degraded in this configuration from $<2\%$ to $\sim 7\%$ rms.

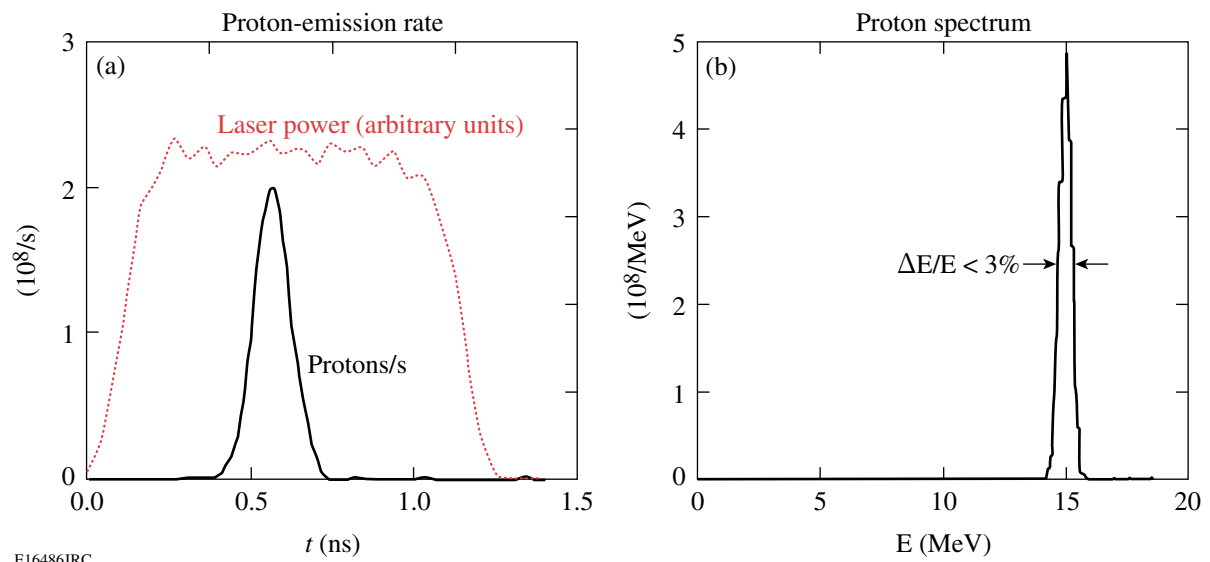


Figure 113.53

Measured characteristics of proton emission from the source implosion. (a) Emission history and (b) spectrum of emitted D^3He protons from the backlighter capsule on OMEGA shot 46531. The total D^3He proton yield was 2.9×10^8 .

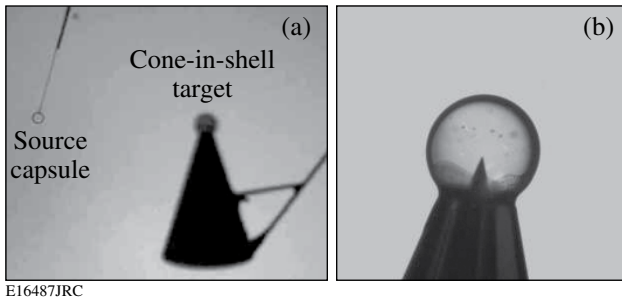


Figure 113.54

(a) Pre-implosion snapshot of source and target capsules. (b) A close-up photograph of the cone-in-shell target sphere. (See also Fig. 113.47.)

The imaging detector is CR-39, a plastic nuclear track detector with submicron spatial resolution, low sensitivity to electromagnetic and x-ray noise sources, and energy-resolving characteristics.²⁶ The position and energy of every incident proton are recorded. The center of the sphere in the subject target is placed 1.0 cm from the center of the backlighter capsule, and the detector is located 25 cm from the source, so structure in the subject is magnified by a factor $M = 25$ at the detector. The relative timing of the backlighter and subject-capsule laser drive beams is adjusted so the backlighter protons arrive at the subject capsule at a desired time interval following the onset of target-capsule drive (Fig. 113.54).

The spatial resolution of the system, neglecting scattering in the target, is limited primarily by the finite source size and results in convolution of structure in the target plane by a Gaussian of about $43\text{-}\mu\text{m}$ FWHM. Smaller structures cannot be observed in the capsule corona without further optimization of the backlighter source.

The energy resolution of the system is about 0.05 MeV, corresponding to an areal-density resolution of about 1.5 mg/cm^2 . A more thorough analysis of the absolute accuracy of proton energy measurements on the radiographic CR-39, as well as an assessment of the effects of angular scattering of protons through plasma in the target plane, is currently in progress.

2. Other Relevant Work

Of direct relevance to this article, and in support of the presence of the observed field structures, Shiraga *et al.*²⁷ and Séguin *et al.*²⁸ inferred the presence of residual electromagnetic fields outside imploded capsules (exploding pushers and ablatively driven implosions similar to those studied here, respectively) on the basis of fluence variations in self-emitted, charged fusion products. Furthermore, character-

ization of capsule assembly and symmetry in ICF-relevant implosions has included extensive use of self-emitted fusion protons,^{26,29} including those from implosions of fast-ignition (FI) targets.³⁰ Recently, Li *et al.*⁷ suggested that a complementary way to study implosions and, in particular, the spatial structure of fields and areal density, is through monoenergetic proton radiography.

Filamentary and jet-like structures were previously observed near the critical surface using shadowgraphic, interferometric, and Faraday rotation techniques by several groups during laser illumination of both planar^{31,32} and spherical targets.^{13,14} As mentioned in the main text, there are substantial differences between the filamentary structures observed by these groups and those reported in this article: (1) The lateral spatial wavelength of structures was $10\text{ }\mu\text{m}$, and examination of their data shows no evidence of the $\sim 150\text{-}\mu\text{m}$ spatial scale that we see. (2) The radial extent of the earlier structures is much smaller and confined, whereas the structures reported here fill the entire field of view. (3) Fine structures originate well into the underdense plasma, while the structures here originate inside the critical surface, even approaching the ablation surface (see Fig. 113.55). (4) For uniformly illuminated implosions, fields greater than 10 T were not detected.³³ In addition, it is useful to point out that one of the unique advantages of the particle probe that we have used is that it is not “cut off” by critical-density plasma effects as is the case for optical probes.

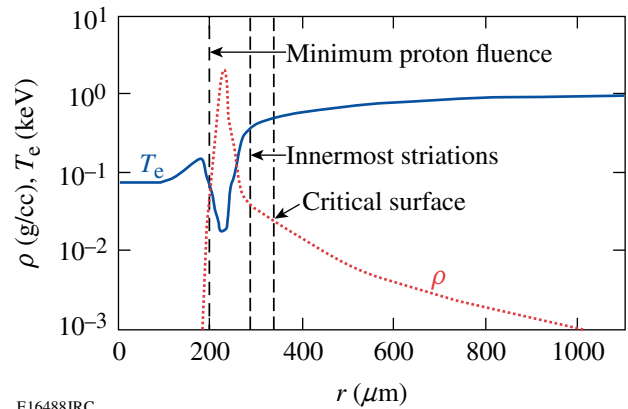


Figure 113.55

LILAC³⁶ simulation of the mass density and electron temperature profiles of the imploding capsule at 1.56 ns, ~ 0.3 ns after the laser has turned off. At this time, the capsule shell (the region of highest density near $230\text{ }\mu\text{m}$) is imploding inward at approximately constant speed. The radius corresponding to the observed minimum proton fluence (Fig. 113.51) occurs at the inner shell surface in the simulation. The innermost striations are observed at about $300\text{ }\mu\text{m}$ [Fig. 113.49(b)], well inside the critical-density surface (for $\lambda = 0.351\text{ }\mu\text{m}$).

Previous studies of laser–capsule interactions using broadband proton radiography³⁴ include Borghesi *et al.*³⁵ and MacKinnon *et al.*¹² Borghesi illuminated a sphere from one side using a short (1 ps), intense pulse and observed filamentary structures similar to those described in the previous paragraph. MacKinnon, however, saw no filamentary or focusing fields surrounding a capsule driven with six 1-ns laser beams. The fact that MacKinnon did not see these structures is not presently understood. There are, however, substantial differences in the implosion conditions compared to the current work. For example, MacKinnon used six beams at 1- μm wavelength and 1.5×10^{13} -W/cm² intensity; herein we used 36 beams at 1/3 μm and 6.7×10^{14} W/cm². In addition, MacKinnon’s radiographic images were obtained substantially after (~ 1.5 ns) the end of the driving laser pulse, whereas in the current work, radiographs were obtained shortly after (~ 0.3 ns) the end of the pulse. If the observed field structures are produced and sustained by the laser (see Possible Mechanisms below), the structures may no longer be detectable 1 ns after their generating source has turned off.

The monoenergetic D³He fusion proton emission from backlighter capsules has, for the purposes of these experiments, distinct advantages over broadband, non-isotropic proton emissions associated with intense-laser-beam experiments.³⁴ A single energy provides unambiguous quantitative relationships between proton energy loss through the target and areal density and also between proton trajectory bending and field strengths at the target. Quasi-isotropy allows for imaging of large objects, or even simultaneous imaging of multiple objects in totally different directions (as has been done in other contexts¹¹).

3. Possible Mechanisms

Numerous instabilities that generate magnetic fields in laser–plasma experiments have been identified or proposed,¹⁷ and take place over a wide range of plasma conditions. Instabilities generated outside the critical surface are the collisionless Weibel, thermomagnetic, and filamentation instabilities. Just inside the critical surface, the collisional Weibel, $\nabla T \times \nabla n$, and thermomagnetic instabilities will grow. Nernst convection can carry B fields generated by these instabilities inward.¹⁷ The electrothermal instability occurs when the mean free path is shorter than the electron skin depth.¹⁹ The Rayleigh–Taylor (RT) instability generates B fields at the ablation front.^{18,20}

Monoenergetic proton radiography of planar foils seeded with RT ripples is currently in progress to investigate the generation and growth of fields by RT processes. Preliminary results have observed ~ 100 -T-magnitude magnetic field struc-

tures, which are absent when the rippled RT seed is absent from the foil.

An estimate of the RT-induced B-field magnitude can be obtained using the work of Nishiguchi.¹⁸ The capsule shell’s acceleration g can be approximated from the experimental observations as the distance the shell has traveled over one half the square of the time it took to get there, $g = 2 \times (430\text{--}215 \mu\text{m}) / (1.5 \text{ ns})^2 \approx 200 \mu\text{m/ns}^2$. The observed transverse spacing between filaments near the capsule surface is typically 150 μm . From *LILAC* simulations,³⁶ $L = 10 \mu\text{m}$ is typical of the plasma density scale length. From these values, $kL = 0.42$. Consulting Fig. 1 of Nishiguchi, this gives a peak B-field magnitude of about 300 T at the end of the linear phase of RT growth—only 5 \times the observed B-field magnitude “averaged” over the width of a filament.

Although RT processes could plausibly generate the observed B fields, other mechanisms cannot yet be ruled out. New experiments using monoenergetic proton radiography will be performed to investigate which instability mechanism(s) is (are) at work. A time sequence of radiographs would enable observation of the onset, growth, and decay of such filamentary structures. Variation of the intensity and other laser conditions could be used to elucidate the origin and any thresholds. Comparison of these radiography results with those from driven solid-CH balls, which undergo no acceleration to drive RT growth, would determine if RT is a dominant mechanism.

Whatever the mechanism, magnetic fields generated close to the ablation front would get “frozen in” to the ablating material and would follow the plasma flow off the capsule surface. Therefore, structures at the edge of the field of view were actually generated some several hundred picoseconds earlier, making it possible to record a history of the filamentary structure in a single radiographic snapshot.

In regard to the coherent focusing field, this article has emphasized the possible and likely connection between the central coherent electric field and the pressure gradient at the fuel–shell interface. Yet, another intriguing consequence is that this field could also opportunistically reflect hot electrons that otherwise might preheat the fuel. To make such an assessment quantitative would require that we have information about both the evolution of this coherent field and how it is affected by the laser pulse shape and the capsule itself. (Because of shot limitations, for example, we have so far investigated only the coherent field for the 1-ns square pulse shape, as depicted in Fig. 113.48.) We would also need rather detailed information

about the bath of hot electrons, how it is generated, how it depends on pulse shape and the capsule, and, in general, how the hot-electron distribution evolves. In the course of exploring the full consequences of the central coherent field, we will investigate this preheat amelioration possibility.

ACKNOWLEDGMENT

We express our gratitude to the OMEGA engineers and operations crew who supported these experiments, and to General Atomics for providing high-quality backlighter and target capsules. This work was supported by the Fusion Science Center (FSC) for Extreme States of Matter and Fast Ignition at the University of Rochester and by the U. S. Department of Energy Office of Inertial Confinement (Grant No. DE-FG03-03NA00058). J. R. R. also acknowledges the FSC for his post-doctoral financial support.

REFERENCES

1. National Research Council (U.S.) Committee on High Energy Density Plasma Physics, *Frontiers in High Energy Density Physics: The X-Games of Contemporary Science* (National Academies Press, Washington, DC, 2003).
2. R. P. Drake, *High-Energy-Density Physics: Fundamentals, Inertial Fusion, and Experimental Astrophysics, Shock Wave and High Pressure Phenomena* (Springer, Berlin, 2006).
3. J. Nuckolls *et al.*, *Nature* **239**, 139 (1972).
4. S. Atzeni and J. Meyer-ter-Vehn, *The Physics of Inertial Fusion: Beam Plasma Interaction, Hydrodynamics, Hot Dense Matter*, International Series of Monographs on Physics (Clarendon Press, Oxford, 2004).
5. B. A. Remington, R. P. Drake, and D. D. Ryutov, *Rev. Mod. Phys.* **78**, 755 (2006).
6. W. L. Kruer, *The Physics of Laser Plasma Interactions, Frontiers in Physics* (Westview Press, Boulder, CO, 2003), pp. 39–43.
7. C. K. Li, F. H. Séguin, J. A. Frenje, J. R. Rygg, R. D. Petrasso, R. P. J. Town, P. A. Amendt, S. P. Hatchett, O. L. Landen, A. J. Mackinnon, P. K. Patel, V. Smalyuk, J. P. Knauer, T. C. Sangster, and C. Stoeckl, *Rev. Sci. Instrum.* **77**, 10E725 (2006).
8. M. Tabak *et al.*, *Phys. Plasmas* **1**, 1626 (1994).
9. R. Kodama *et al.*, *Nature* **418**, 933 (2002).
10. C. K. Li, F. H. Séguin, J. A. Frenje, J. R. Rygg, R. D. Petrasso, R. P. J. Town, P. A. Amendt, S. P. Hatchett, O. L. Landen, A. J. Mackinnon, P. K. Patel, V. A. Smalyuk, T. C. Sangster, and J. P. Knauer, *Phys. Rev. Lett.* **97**, 135003 (2006).
11. C. K. Li, F. H. Séguin, J. A. Frenje, J. R. Rygg, R. D. Petrasso, R. P. J. Town, O. L. Landen, J. P. Knauer, and V. A. Smalyuk, *Phys. Rev. Lett.* **99**, 055001 (2007).
12. A. J. Mackinnon *et al.*, *Phys. Rev. Lett.* **97**, 045001 (2006).
13. T. Mochizuki *et al.*, *Jpn. J. Appl. Phys.* **19**, L645 (1980).
14. O. Willi and P. T. Rumsby, *Opt. Commun.* **37**, 45 (1981).
15. C. K. Li and R. D. Petrasso, *Phys. Rev. Lett.* **70**, 3059 (1993).
16. Numerical simulations of full-sphere capsules, equivalent to the target capsule with no cone, were performed with the 1-D hydrodynamic code *LILAC*.³⁶ The use of 1-D spherical geometry to simulate the areal density of cone-in-shell capsules was previously used and found reasonable.³⁰
17. M. G. Haines, *Can. J. Phys.* **64**, 912 (1986).
18. A. Nishiguchi, *Jpn. J. Appl. Phys.* **41**, 326 (2002).
19. M. G. Haines, *Phys. Rev. Lett.* **47**, 917 (1981).
20. K. Mima, T. Tajima, and J. N. Leboeuf, *Phys. Rev. Lett.* **41**, 1715 (1978).
21. The filamentary and focusing fields are present irrespective of whether the capsule is of the hot-spot or fast-ignition variety.
22. T. R. Boehly, D. L. Brown, R. S. Craxton, R. L. Keck, J. P. Knauer, J. H. Kelly, T. J. Kessler, S. A. Kumpan, S. J. Loucks, S. A. Letzring, F. J. Marshall, R. L. McCrory, S. F. B. Morse, W. Seka, J. M. Soares, and C. P. Verdon, *Opt. Commun.* **133**, 495 (1997).
23. S. Skupsky and R. S. Craxton, *Phys. Plasmas* **6**, 2157 (1999).
24. J. A. Frenje, C. K. Li, F. H. Séguin, J. Deciantis, S. Kurebayashi, J. R. Rygg, R. D. Petrasso, J. Delettrez, V. Yu. Glebov, C. Stoeckl, F. J. Marshall, D. D. Meyerhofer, T. C. Sangster, V. A. Smalyuk, and J. M. Soares, *Phys. Plasmas* **11**, 2798 (2003).
25. Hot electrons escaping from the backlighter capsule during laser irradiation results in a capsule charge of several hundred kV, which accelerates the escaping D³He protons above their 14.7-MeV birth energy. This shift is measured to 0.1-MeV accuracy by the proton spectrometers.²⁶
26. F. H. Séguin, J. A. Frenje, C. K. Li, D. G. Hicks, S. Kurebayashi, J. R. Rygg, B.-E. Schwartz, R. D. Petrasso, S. Roberts, J. M. Soares, D. D. Meyerhofer, T. C. Sangster, J. P. Knauer, C. Sorce, V. Yu. Glebov, C. Stoeckl, T. W. Phillips, R. J. Leeper, K. Fletcher, and S. Padalino, *Rev. Sci. Instrum.* **74**, 975 (2003).
27. H. Shiraga, T. Mochizuki, and C. Yamanaka, *Appl. Phys. Lett.* **37**, 602 (1980).
28. F. H. Séguin, C. K. Li, J. A. Frenje, S. Kurebayashi, R. D. Petrasso, F. J. Marshall, D. D. Meyerhofer, J. M. Soares, T. C. Sangster, C. Stoeckl, J. A. Delettrez, P. B. Radha, V. A. Smalyuk, and S. Roberts, *Phys. Plasmas* **9**, 3558 (2002).
29. H. Azechi *et al.*, *Laser Part. Beams* **9**, 193 (1991).
30. C. Stoeckl, T. R. Boehly, J. A. Delettrez, S. P. Hatchett, J. A. Frenje, V. Yu. Glebov, C. K. Li, J. E. Miller, R. D. Petrasso, F. H. Séguin, V. A. Smalyuk, R. B. Stephens, W. Theobald, B. Yaakobi, and T. C. Sangster, *Plasma Phys. Control. Fusion* **47**, B856 (2005).
31. B. Grek *et al.*, *Phys. Rev. Lett.* **41**, 1811 (1978).

32. G. Thiell and B. Meyer, *Laser Part. Beams* **3**, 51 (1985).
33. O. Willi, P. T. Rumsby, and C. Duncan, *Opt. Commun.* **37**, 40 (1981).
34. A. J. Mackinnon, P. K. Patel, R. P. Town, M. J. Edwards, T. Phillips, S. C. Lerner, D. W. Price, D. Hicks, M. H. Key, S. Hatchett, S. C. Wilks, M. Borghesi, L. Romagnani, S. Kar, T. Toncian, G. Pretzler, O. Willi, M. Koenig, E. Martinolli, S. Lepape, A. Benuzzi-Mounaix, P. Audebert, J. C. Gauthier, J. King, R. Snavely, R. R. Freeman, and T. Boehly, *Rev. Sci. Instrum.* **75**, 3531 (2004).
35. M. Borghesi *et al.*, *Phys. Plasmas* **9**, 2214 (2002).
36. J. Delettrez, R. Epstein, M. C. Richardson, P. A. Jaanimagi, and B. L. Henke, *Phys. Rev. A* **36**, 3926 (1987).

